CHEMISTRY OF MATERIALS

Communication

pubs.acs.org/cm

Red-to-Black Piezochromism in a Compressible Pb−I−SCN Layered Perovskite

Daiki Umeyama,[†] Yu Lin,[†,‡,§] and Hemamala I. Karunadasa*[,†]

[†]Departments of Chemistry and [‡]Geological Sciences, Stanford University, Stanford, California 94305, United States

[§]Stanford Institute for Materials and Energy Sciences, SLAC National Accelerator Laboratory, Menlo Park, California 94025, United States

Supporting Information

Means of controlling semiconductor bandgaps are of great importance in materials design. In particular, fabrication of layered heterostructures with controlled thickness and composition allows for the composite's electronic structures to be modulated.[1] In recent decades, 2D organic−inorganic perovskites have gained attention as self-assembling heterostructures, whose optoelectronic properties can be tuned through crystal design. Indeed, hybrid perovskites have proven to be a versatile platform for optoelectronics. The high bandgaps (E_g) and large exciton binding energies (E_b) in n = 1 lead-halide perovskites (n = number of lead-halide sheets in each inorganic layer) have aided their application as green light-emitting diodes[2,3] and white-light phosphors.[4,5] In contrast, the much lower E_g and E_b values in the 3D (n = ∞) perovskite $(MA)PbI_3$ (MA = $CH_3NH_3^+$) have been critical for its successful employment as an absorber for high-efficiency solar cells.[6,7] Both E_g and E_b values of 2D perovskites decrease with increasing inorganic sheet thickness.[8,9] Accordingly, the n = 3 perovskite $(C_6H_5(CH_2)_2NH_3)_2(MA)_2[Pb_3I_{10}]$ was shown to act as an absorber in a solar cell with improved moisture resistance compared to $(MA)PbI_3$.[10] However, self-assembly of single-phased n > 1 perovskites becomes more difficult as n increases.[9] We therefore explored routes to n = 1 structures with reduced E_g and E_b values. Herein we show that $(MA)_2[PbI_2(SCN)_2]$ (**1**) has atypically low E_g and E_b values for an n = 1 perovskite and dramatic pressure response (Figure 1) that further modulates its photophysical properties.

Recently, a proposed analog to the 3D perovskite $(MA)PbI_3$ was reported where two iodides were replaced by two thiocyanides.[11] This material was reported to exhibit greater moisture resistance compared to $(MA)PbI_3$ and similar performance as a solar-cell absorber. A recent correspondence[12] reported its single-crystal structure as the 2D perovskite **1** containing bridging iodides and terminal thiocyanides. Solid **1** has been attributed an E_g of 1.5−1.6 eV, similar to that of $(MA)PbI_3$, which would be promising for photovoltaic applications.[11−13] Several reports of mixed Pb−I−SCN perovskite absorbers have also ascribed increased photoluminescence (PL) intensity[14,15] and improved device performance and stability[14] to SCN^- incorporation. In our hands, however, we find that the red solid **1**, which has an E_g of ca. 2.3 eV (Figure 2A), rapidly decomposes to a black solid in ambient humidity. Upon exposing **1** to 66% relative humidity, we see reflections corresponding to $(MA)PbI_3$ and $Pb(SCN)_2$ in the powder X-ray diffraction (PXRD) patterns, which dominate the patterns after 7 min for films and 45 min for powders (Figure S1). The

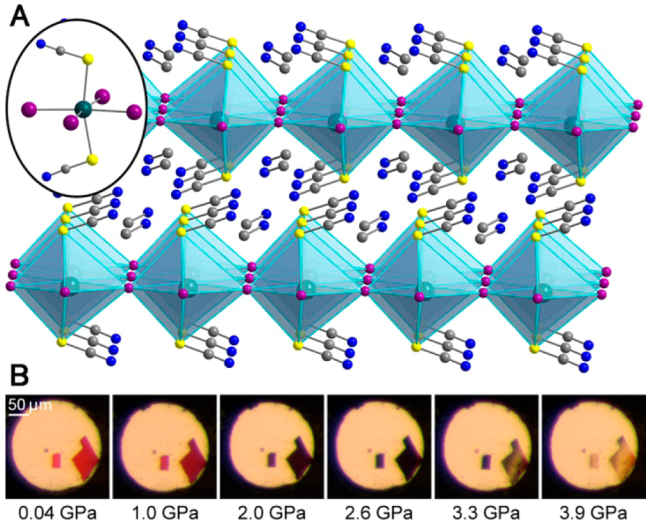

Figure 1. (A) Crystal structure of $(CH_3NH_3)_2[PbI_2(SCN)_2]$ (**1**).[12] Turquoise, purple, yellow, blue, and gray spheres represent Pb, I, S, N, and C atoms, respectively. H atoms omitted for clarity. Inset: the Pb^{2+} coordination sphere. (B) Piezochromism in single crystals of **1**.

absorption, PL, and vibrational spectra of humidity-exposed **1** also show indicators for $(MA)PbI_3$ formation (Figures S2−S5), which may explain the low E_g and favorable photovoltaic properties previously attributed to **1**. Considering stoichiometry, the following decomposition mechanism is possible, driven by the hydration of (MA)SCN.

$$3(MA)_2[PbI_2(SCN)_2] \rightarrow 2(MA)PbI_3 + 4(MA)SCN + Pb(SCN)_2$$

All manipulations with **1** described below were therefore conducted under dry conditions. Annealing **1** above 50 °C also converts it to a black solid, whose XRD peaks match those of $(MA)PbI_3$ and $Pb(SCN)_2$ (Figures S6 and S7). Further discussion and characterization of the decomposition products are provided in the Supporting Information. We note that just prior to submission of this paper, the bandgap of **1** was reported by Yan, Mitzi et al. to be 2.0−2.1 eV,[16] which

Received: March 22, 2016
Revised: May 7, 2016

DOI: 10.1021/acs.chemmater.6b01147
Chem. Mater. XXXX, XXX, XXX−XXX

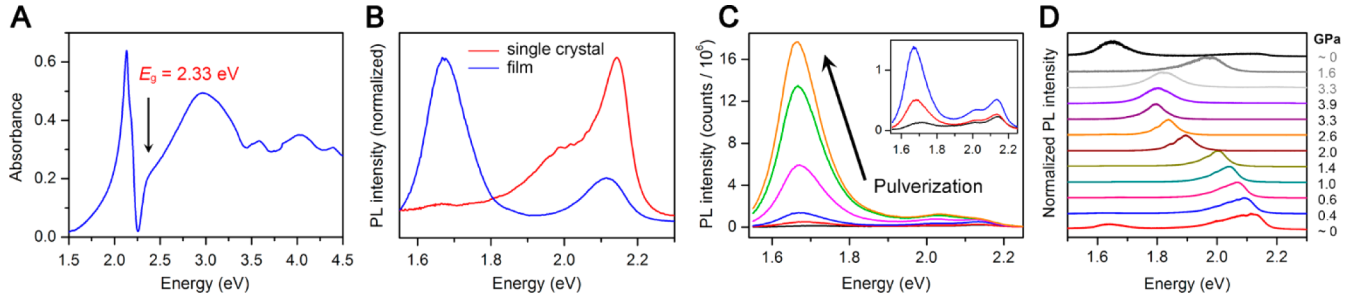

Figure 2. (A) Optical absorption spectrum of a **1** film at 6 K. (B) Photoluminescence (PL) spectra from a single crystal (red) and a film (blue) of **1**. (C) PL from **1** crystals as a function of grinding. (D) Single-crystal PL of **1** upon compression (colored) and decompression (grayscale) in a diamond-anvil cell.

independently confirms that the material's E_g is higher than previously thought.

Combining dimethylformamide (DMF) solutions of $Pb(SCN)_2$ and (MA)I initially affords yellow needles of the 1D structure $(MA)_2[Pb_3I_8(DMF)_2]$ (Figure S8). Further evaporation of DMF yields **1** crystals as previously described.[12] Diffusion of diethyl ether into a tetrahydrofuran solution of the precursors affords higher-quality **1** crystals, which we used for optical and diffraction studies. Interestingly, compared to the separation between inorganic layers in the 77 reported (001) n = 1 Pb−I perovskites in the Cambridge Structural Database that range from 32.2 to 10.1 Å, **1** has the shortest interlayer distance of 9.2901(9) Å. The 300 K structure of **1** also shows an interlayer S−S distance of 5.182(6) Å. Furthermore, unlike in most 2D perovskites, all Pb and bridging I atoms in **1** reside on the same plane, with no out-of-plane octahedral tilting and minimal in-plane octahedral tilting (average in-plane Pb−I−Pb angle of 171.57(8)°). Octahedral tilting in 2D perovskites has been attributed to hydrogen bonds between NH_3 groups and halides.[17] In **1**, each NH_3 group forms hydrogen bonds with the nitrogen ends of two SCN^- ligands in adjacent sheets and with one iodide, allowing for flatter inorganic sheets. These structural changes, compared to typical n = 1 perovskites, manifest in **1**'s optical properties.

Absorption spectra of layered perovskites show a step denoting their bandgap onsets, owing to their 2D density of states.[8,18] The 6 K optical absorbance spectrum of a **1** film shows a sharp excitonic absorption at 2.13 eV and the expected step-shaped bandgap onset (Figure 2A). This step in the low-temperature absorption spectrum allows us to estimate the E_g as 2.33 eV. The exciton's high oscillator strength and broadening at higher temperatures obscure this step in the room-temperature absorption data. However, the excitonic absorption energies in the room-temperature and 6 K absorption spectra differ by only 0.05 eV (Figure S9A), indicating that the bandgaps should also be similar at these temperatures. Furthermore, we do not see sharp transitions in **1**'s PL energy between 18 and 200 K (Figure S9B), suggesting the absence of first-order phase transitions within this temperature regime. We can then estimate E_b as 200 meV ($E_b = E_g$ − exciton absorption energy).[8] These E_g and E_b values are low for an n = 1 Pb−I perovskite and are intermediate to those of n = 2 and 3 perovskites. For example, the n = 1 perovskite $(C_6H_{13}NH_3)_2[PbI_4]$ has a reported E_g of 2.70 eV and E_b of 361 meV, whereas its n = 2 and 3 analogs, $(C_6H_{13}NH_3)_2(MA)_{n-1}[Pb_nI_{3n+1}]$, are reported to have E_g values of 2.40 and 2.17 eV, and E_b values of 260 and 150 meV, respectively.[19] The n = 1 perovskite $(C_6H_5(CH_2)_2NH_3)_2[PbI_4]$ is reported to have a low E_b of 220 meV, attributed to the increased dielectric constant of the aromatic groups,[20] although its E_g of 2.58 eV is larger than that of **1**.

The short interlayer distance likely contributes to the small E_g and E_b values in **1**. Decreasing the interlayer spacing in 2D perovskites has been shown to reduce the confinement of the inorganic sheets.[21,22] Low exciton peak energies of ca. 2.3 eV have been reported in 2D perovskites with short interlayer spacing.[23] Reduced octahedral tilting in the inorganic sheets has also been correlated with an E_g reduction in these materials.[17,24] The covalency of the Pb−S linkages may also allow for some delocalization of the π electrons in the SCN^- ligands. This could increase the polarizability of the inorganic sheets, thereby decreasing its dielectric confinement[8,25] and E_b.

We then obtained PL spectra on single crystals of **1**. Excitation at 375 nm yields intense PL at 2.14 eV with a shoulder at 2.00 eV (Figure 2B). Another PL feature also appears at 1.68 eV. The intensities of these bands vary between crystals and between locations in a single crystal (Figure S10). PL spectra of **1** films show the same features, but with very different relative intensities. In films the lower-energy PL peak is dominant and the higher-energy peak shows much weaker intensity (Figure 2B). The higher-energy PL is likely from excitonic emission with a Stokes shift of ca. 70 meV at 300 K (Figure S11A). However, the origin of the lower-energy PL is less clear. Its greatly reduced intensity in crystals compared to films suggests that particle surfaces, defects or impurities contribute to the emission. The excitation spectrum of this lower-energy PL resembles the absorption spectrum of **1** and does not show significant absorption at 1.6 eV where we expect any $(MA)PbI_3$ impurity to absorb (Figure S11B). We further monitored the PL of **1** crystals as they were pulverized in a dry N_2 atmosphere. We see the intensity of the low-energy PL (which was initially weaker than the high-energy PL) greatly increase with extended material grinding (Figure 2C). This suggests an origin from defects at particle surfaces or in the bulk, although we cannot eliminate $(MA)PbI_3$ impurity from contributing to this low-energy PL by serving as recombination trap states.

Because the MA cations are buried within the $[PbI_2(SCN)_2]^{2-}$ layers that do not interdigitate, we investigated if pressure could change **1**'s optical properties. Indeed, upon compression below 1 GPa in a diamond-anvil cell, a translucent red single crystal of **1** begins to darken and it turns opaque black at 2.6 GPa, suggesting a substantial decrease in bandgap (Figure 1B). Upon further compression the crystal becomes translucent yellow at 3.9 GPa and this color is retained up to 4.3 GPa. Notably, these color changes are fully reversible upon

DOI: 10.1021/acs.chemmater.6b01147
Chem. Mater. XXXX, XXX, XXX−XXX

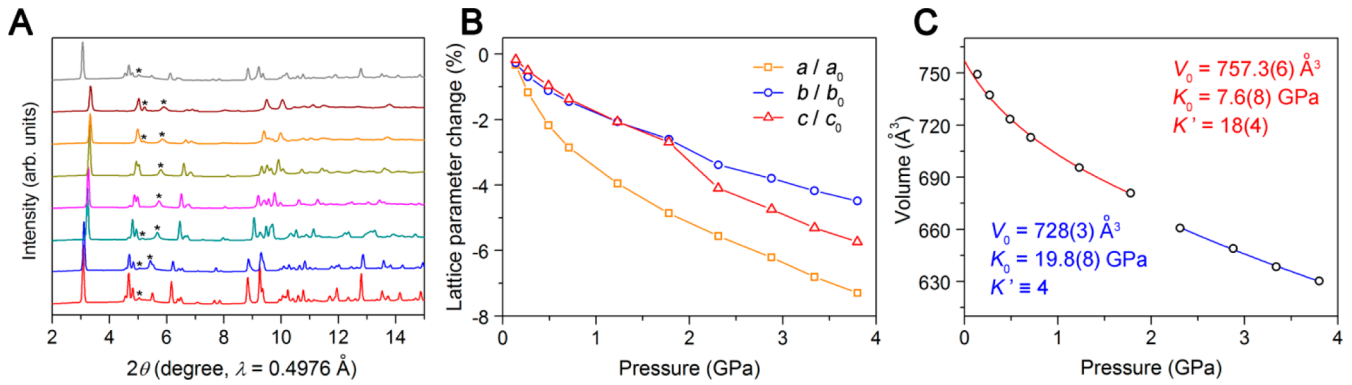

Figure 3. (A) PXRD patterns of **1** upon compression up to 5.7 GPa (red to brown) and decompression to ambient pressure (gray). Asterisks denote reflections from the pressure medium. (B) Lattice-parameter evolution with pressure. (C) Unit-cell volume changes with pressure with third- (red) and second-order (blue) Birch–Murnaghan fits.

decompression (Figure S12). Upon compression to 2.6 GPa, the PL of a single crystal shows the major high-energy PL band gradually redshift from 2.1 to 1.8 eV (Figure 2D). The minor PL band at 1.6 eV decreases in intensity with compression and disappears above 2.0 GPa (Figure S13). Interestingly, the energy shifts of this minor PL band with pressure (Figure S13) are similar to those seen in the PL energy of $(MA)PbI_3$ with compression,[26] suggesting that it may originate from a trace amount of the 3D perovskite. Assuming no change in Stokes shift and E_b within this pressure range, we estimate the E_g at 2.6 GPa to decrease by 0.3 eV. Thus, relatively low pressure affords an E_g of ca. 2.0 eV. The black color of **1** at 2.6 GPa suggests that the E_g value may be still lower than this estimate. Although similar piezochromic transitions (from yellow to black) have been observed in 2D Cu–Cl perovskites, these occur at much higher pressures of ca. 12 GPa.[27] High-pressure studies on 2D Pb–I perovskites have shown a decrease in E_g to ca. 2 eV, although this occurs at very high pressures exceeding 24 GPa.[28] Therefore, **1** has a significantly greater pressure response compared to typical n = 1 perovskites.

To probe the structural basis for **1**'s pressure response, we collected high-pressure PXRD patterns of **1** powder. The reversible color changes seen in the crystal were also evident in the powder, albeit with a slight difference in the black-to-yellow transition pressure (Figure S14). The reflections up to 3.8 GPa could be indexed to the original space group ($Pmn2_1$) to obtain lattice parameters (Figure 3A). The crystallographic a axis (layer stacking direction) is monotonically compressed by 7.3% from 0 to 3.8 GPa, reducing the interlayer distance from 9.29 to 8.61 Å (Figure 3B). The b and c axes show a lesser contraction below 2 GPa, followed by a pronounced discontinuity in the c-axis length and unit-cell volume at 2.3 GPa, suggesting a phase transition. Space-group assignments above 2.3 GPa are less reliable because of pressure-induced line broadening and overlapping Bragg peaks and **1** begins to amorphize above 3.8 GPa. The reflections in the original PXRD pattern are regained upon decompression to ambient pressure. The volume variation below 2 GPa was fit by the third-order Birch–Murnaghan equation of state (BM EOS) to yield a low K_0 (ambient-pressure bulk modulus) of 7.6(8) GPa and a K' (pressure derivative of K_0) of 18(4) (Figure 3C). These values indicate that **1** is highly compressible near ambient pressure but rapidly stiffens with compression. Such small K_0 and large deviation of K' from 4 are more commonly seen in molecular solids.[29] The volume change above 2 GPa was well fit by the second-order BM EOS (K_0 = 19.8(8) GPa and $K' \equiv 4$), indicating that **1** is much less compressible after the phase transition. Layered materials such as graphite and transition metal dichalcogenide intercalation compounds show similar anisotropic compressibility with greater lattice contraction along the layer stacking direction, although these materials have much higher K_0 values.[30,31]

Solid **1** displays low E_g and E_b values for an n = 1 perovskite. However, **1** must be handled carefully. The E_g of 1.6 eV previously assigned to this material may be due to its rapid decomposition under humid conditions or annealing temperatures to form $(MA)PbI_3$. The hybrid is highly compressible with the interlayer distance contracting by ca. 2% per GPa from 0 to 3.8 GPa. This affords striking piezochromism from red to black to yellow. We estimate that **1**'s E_g decreases to ca. 2.0 eV upon compression to 2.6 GPa. The atypical optical properties of **1** and its large pressure response may originate from the short interlayer contact as well as the covalency of the Pb–S linkages. The electronic effects of SCN^- substitution in the Pb–I lattice, as well as the material's substantial response to relatively modest pressures, provide new routes for achieving further optical and electronic diversity from 2D perovskites.

■ ASSOCIATED CONTENT

Supporting Information

The CIF for $(MA)_2[Pb_3I_8(DMF)_2]$ has been deposited in the Cambridge Crystallographic Data Centre, deposition number: 1469899. The Supporting Information is available free of charge on the ACS Publications website at DOI: 10.1021/acs.chemmater.6b01147.

Experimental and crystallographic details and spectra (PDF).

Crystallographic data in cif format (CIF).

■ AUTHOR INFORMATION

Corresponding Author

*H. I. Karunadasa. E-mail: hemamala@stanford.edu.

Funding

This research was funded by the NSF CAREER award DMR-1351538 and the Global Climate and Energy Project.

Notes

The authors declare no competing financial interest.

DOI: 10.1021/acs.chemmater.6b01147
Chem. Mater. XXXX, XXX, XXX–XXX

■ ACKNOWLEDGMENTS

D.U. is supported by a postdoctoral fellowship from the Japanese Society for the Promotion of Science. XRD studies were done at the Stanford Nanocharacterization Laboratory. High-pressure XRD experiments were performed at the Advanced Light Source (ALS) beamline 12.2.2. The ALS is supported by the Director, Office of Science, Office of Basic Energy Sciences, of the U.S. Department of Energy under Contract No. DE-AC02-05CH11231. We thank Profs. E. I. Solomon, M. D. McGehee, and W. L. Mao for access to equipment.

■ REFERENCES

(1) Esaki, L. A Bird's-Eye View on the Evolution of Semiconductor Superlattices and Quantum Wells. *IEEE J. Quantum Electron.* **1986**, *22*, 1611.

(2) Hattori, T.; Taira, T.; Era, M.; Tsutsui, T.; Saito, S. Highly Efficient Electroluminescence from a Heterostructure Device Combined with Emissive Layered-Perovskite and an Electron-Transporting Organic Compound. *Chem. Phys. Lett.* **1996**, *254*, 103.

(3) Chondroudis, K.; Mitzi, D. B. Electroluminescence from an Organic−Inorganic Perovskite Incorporating a Quaterthiophene Dye within Lead Halide Perovskite Layers. *Chem. Mater.* **1999**, *11*, 3028.

(4) Dohner, E. R.; Hoke, E. T.; Karunadasa, H. I. Self-Assembly of Broadband White-Light Emitters. *J. Am. Chem. Soc.* **2014**, *136*, 1718.

(5) Dohner, E. R.; Jaffe, A.; Bradshaw, L. R.; Karunadasa, H. I. Intrinsic White-Light Emission from Layered Hybrid Perovskites. *J. Am. Chem. Soc.* **2014**, *136*, 13154.

(6) Kojima, A.; Teshima, K.; Shirai, Y.; Miyasaka, T. Organometal Halide Perovskites as Visible-Light Sensitizers for Photovoltaic Cells. *J. Am. Chem. Soc.* **2009**, *131*, 6050.

(7) Green, M. A.; Ho-Baillie, A.; Snaith, H. J. The Emergence of Perovskite Solar Cells. *Nat. Photonics* **2014**, *8*, 506.

(8) Ishihara, T. Optical Properties of PbI-Based Perovskite Structures. *J. Lumin.* **1994**, *60−61*, 269.

(9) Mitzi, D. B.; Feild, C. A.; Harrison, W. T. A.; Guloy, A. M. Conducting Tin Halides with a Layered Organic-Based Perovskite Structure. *Nature* **1994**, *369*, 467.

(10) Smith, I. C.; Hoke, E. T.; Solis-Ibarra, D.; McGehee, M. D.; Karunadasa, H. I. A Layered Hybrid Perovskite Solar-Cell Absorber with Enhanced Moisture Stability. *Angew. Chem., Int. Ed.* **2014**, *53*, 11232.

(11) Jiang, Q.; Rebollar, D.; Gong, J.; Piacentino, E. L.; Zheng, C.; Xu, T. Pseudohalide-Induced Moisture Tolerance in Perovskite $CH_3NH_3Pb(SCN)_2I$ Thin Films. *Angew. Chem., Int. Ed.* **2015**, *54*, 7617.

(12) Daub, M.; Hillebrecht, H. Synthesis, Single-Crystal Structure and Characterization of $(CH_3NH_3)_2Pb(SCN)_2I_2$. *Angew. Chem., Int. Ed.* **2015**, *54*, 11016.

(13) Ganose, A. M.; Savory, C. N.; Scanlon, D. O. $(CH_3NH_3)_2Pb(SCN)_2I_2$: A More Stable Structural Motif for Hybrid Halide Photovoltaics? *J. Phys. Chem. Lett.* **2015**, *6*, 4594.

(14) Chen, Y.; Li, B.; Huang, W.; Gao, D.; Liang, Z. Efficient and Reproducible $CH_3NH_3PbI_{3-x}(SCN)_x$ Perovskite Based Planar Solar Cells. *Chem. Commun.* **2015**, *51*, 11997.

(15) Halder, A.; Chulliyil, R.; Subbiah, A. S.; Khan, T.; Chattoraj, S.; Chowdhury, A.; Sarkar, S. K. Pseudohalide (SCN^-)-Doped $MAPbI_3$ Perovskites: A Few Surprises. *J. Phys. Chem. Lett.* **2015**, *6*, 3483.

(16) Xiao, Z.; Meng, W.; Saparov, B.; Duan, H.-S.; Wang, C.; Feng, C.; Liao, W.; Ke, W.; Zhao, D.; Wang, J.; Mitzi, D. B.; Yan, Y. Photovoltaic Properties of Two-Dimensional $(CH_3NH_3)_2Pb(SCN)_2I_2$ Perovskite: A Combined Experimental and Density Functional Theory Study. *J. Phys. Chem. Lett.* **2016**, *7*, 1213.

(17) Sourisseau, S.; Louvain, N.; Bi, W.; Mercier, N.; Rondeau, D.; Boucher, F.; Buzaré, J.-Y.; Legein, C. Reduced Band Gap Hybrid Perovskites Resulting from Combined Hydrogen and Halogen Bonding at the Organic−Inorganic Interface. *Chem. Mater.* **2007**, *19*, 600.

(18) Hong, X.; Ishihara, T.; Nurmikko, A. V. Photoconductivity and Electroluminescence in Lead Iodide Based Natural Quantum Well Structures. *Solid State Commun.* **1992**, *84*, 657.

(19) Kenichiro, T.; Takashi, K. Bandgap and Exciton Binding Energies in Lead-Iodide-Based Natural Quantum-Well Crystals. *Sci. Technol. Adv. Mater.* **2003**, *4*, 599.

(20) Hong, X.; Ishihara, T.; Nurmikko, A. V. Dielectric Confinement Effect on Excitons in PbI_4-Based Layered Semiconductors. *Phys. Rev. B: Condens. Matter Mater. Phys.* **1992**, *45*, 6961.

(21) Tanaka, K.; Takahashi, T.; Kondo, T.; Umeda, K.; Ema, K.; Umebayashi, T.; Asai, K.; Uchida, K.; Miura, N. Electronic and Excitonic Structures of Inorganic-Organic Perovskite-Type Quantum-Well Crystal $(C_4H_9NH_3)_2PbBr_4$. *Jpn. J. Appl. Phys.* **2005**, *44*, 5923.

(22) Takagi, H.; Kunugita, H.; Ema, K. Influence of the Image Charge Effect on Excitonic Energy Structure in Organic-Inorganic Multiple Quantum Well Crystals. *Phys. Rev. B: Condens. Matter Mater. Phys.* **2013**, *87*, 125421.

(23) Mercier, N.; Poiroux, S.; Riou, A.; Batail, P. Unique Hydrogen Bonding Correlating with a Reduced Band Gap and Phase Transition in the Hybrid Perovskites $(HO(CH_2)_2NH_3)_2PbX_4$ (X = I, Br). *Inorg. Chem.* **2004**, *43*, 8361.

(24) Mitzi, D. B.; Dimitrakopoulos, C. D.; Kosbar, L. L. Structurally Tailored Organic−Inorganic Perovskites: Optical Properties and Solution-Processed Channel Materials for Thin-Film Transistors. *Chem. Mater.* **2001**, *13*, 3728.

(25) Pedesseau, L.; Jancu, J.-M.; Rolland, A.; Deleporte, E.; Katan, C.; Even, J. Electronic Properties of 2D and 3D Hybrid Organic/Inorganic Perovskites for Optoelectronic and Photovoltaic Applications. *Opt. Quantum Electron.* **2014**, *46*, 1225.

(26) Jaffe, A.; Lin, Y.; Beavers, C. M.; Voss, J.; Mao, W. L.; Karunadasa, H. I. High-Pressure Single-Crystal Structures of 3D Lead-Halide Hybrid Perovskites and Pressure Effects on Their Electronic and Optical Properties. *ACS Cent. Sci.* **2016**, *2*, 201.

(27) Jaffe, A.; Lin, Y.; Mao, W. L.; Karunadasa, H. I. Pressure-Induced Conductivity and Yellow-to-Black Piezochromism in a Layered Cu−Cl Hybrid Perovskite. *J. Am. Chem. Soc.* **2015**, *137*, 1673.

(28) Matsuishi, K.; Suzuki, T.; Onari, S.; Gregoryanz, E.; Hemley, R. J.; Mao, H. K. Excitonic States of Alkylammonium Lead-Iodide Layered Perovskite Semiconductors under Hydrostatic Pressure to 25 GPa. *Phys. Status Solidi B* **2001**, *223*, 177.

(29) Vaidya, S. N.; Kennedy, G. C. Compressibility of 18 Molecular Organic Solids to 45 kbar. *J. Chem. Phys.* **1971**, *55*, 987.

(30) Ehm, L.; Knorr, K.; Peters, L.; Rath, S.; Depmeier, W. Pressure Induced Phase Transition in $Fe_{0.47}NbS_2$ Studied by Powder X-Ray Diffraction. *J. Alloys Compd.* **2007**, *429*, 82.

(31) Clarke, R.; Uher, C. High Pressure Properties of Graphite and Its Intercalation Compounds. *Adv. Phys.* **1984**, *33*, 469.

DOI: 10.1021/acs.chemmater.6b01147
Chem. Mater. XXXX, XXX, XXX−XXX